



Deliverable 2.1: Framework for forward modelling of the DigiMon data

DigiMon

Digital monitoring of CO₂ storage projects

Prepared by:

Vincent Vandeweyer^a, Bob Paap^a, Thibault Candela^a, Tuhin Bhakta^b, Martha Lien^c

^aTNO

^bNORCE

^cOctio Environmental

Revision

Version	Date	Change	Page
1.0	03-05-2021	First version	All
1.1	17-05-2021	QA version comments	All
2.1	08-06-2021	Edited version	All

Document distribution

ACT Coordinator

- Research Council of Norway

ACT national funding agencies

- Forschungszentrum Jülich GmbH, Projektträger Jülich, (FZJ/PtJ), Germany.
- Geniki Grammatia Erevnas kai Technologias/The General Secretariat for Research and Technology (GSRT), Greece.
- Ministry of Economic Affairs and Climate/Rijksdienst voor Ondernemend Nederland (RVO), the Netherlands.
- The Research Council of Norway (RCN), Norway.
- Gassnova, Norway.
- Development and Executive Agency for Higher Education, Research, Development and Innovation Funding (UEFISCDI), Romania.
- Department for Business, Energy and Industrial Strategy (BEIS), UK.
- Department of Energy (DoE), USA.

DigiMon partners

- NORCE Norwegian Research Centre AS
- OCTIO Environmental Monitoring AS
- NTNU Norwegian University of Science and Technology
- University of Bristol
- CRES Centre for Renewable Energy Sources and Saving
- Helmholtz–Centre for Environmental Research
- Sedona Development SRL
- TNO Nederlandse Organisatie voor toegepast -natuurwetenschappelijk Onderzoek
- Geotomographie GmbH
- LLC Lawrence Livermore National Security
- SILIXA LTD
- EQUINOR ASA
- REPSOL –NORGE AS

Table of contents

Revision	2
Document distribution	3
Table of contents	4
1 Introduction	5
2 Approach	7
2.1 <i>Links to other WP's</i>	7
3 Modelling Framework	9
3.1 <i>Gravity modelling</i>	9
3.2 <i>Ground movement modelling</i>	12
3.3 <i>Seismic and DAS modelling</i>	14
3.4 <i>Fault stability modelling</i>	17
3.5 <i>Dynamic flow modelling</i>	18
4 Towards field cases	20
4.1 <i>Gravity and ground movement modelling</i>	21
4.2 <i>Seismic and DAS modelling</i>	24
4.3. <i>Fault stability modelling</i>	30
5 Conclusions	32
6 References	33

1 Introduction

Deliverable D2.1 adds to the main goal of WP2 of the ACT DigiMon project, which is to develop the integrated DigiMon system. The key target for WP2 is to optimally integrate various system components into a reliable and usable system.

This deliverable (D2.1) describes the key forward modelling tools of the DigiMon monitoring system. In particular, the modelling tools required to simulate the data response for the individual DigiMon system components that is; Distributed Acoustic Sensing (DAS), conventional seismic, 4D gravity data, and seafloor deformation.

Focus was put on general usability of modelling activities for monitoring of an offshore CO₂ injection site. This infers that the models should be complex enough to cover all the essential parameters, but on the other hand be fast and light enough to run on currently available hardware.

The framework described in this deliverable does not focus on detailed modelling for very specific processes, e.g. the analysis of the transfer function in DAS measurements. But it does take into account the general usability of modelling tools for follow-up activities, like ensemble based inversion and system optimization workflows.

This deliverable results from part of the work defined in task 2.2: “Setting up forward modelling framework at selected CCS sites”. In this task we lay the foundations for the modelling frameworks

Figure 1) to be employed in task 2.4 - “Integrated interpretation and uncertainty quantification”, where it is planned to implement individual forward models and couple these to a dynamic flow simulator in an ensemble-based inversion framework. Perform Inverse modelling studies with individual and multiple data components and task 2.6 - “Optimize the monitoring solution”, where work will be done to optimization of the monitoring solution will be based on a Bayesian framework, obtaining information obtained through the TRA and SEL analysis for the different system components, combined with a dedicated uncertainty quantification of the system components.

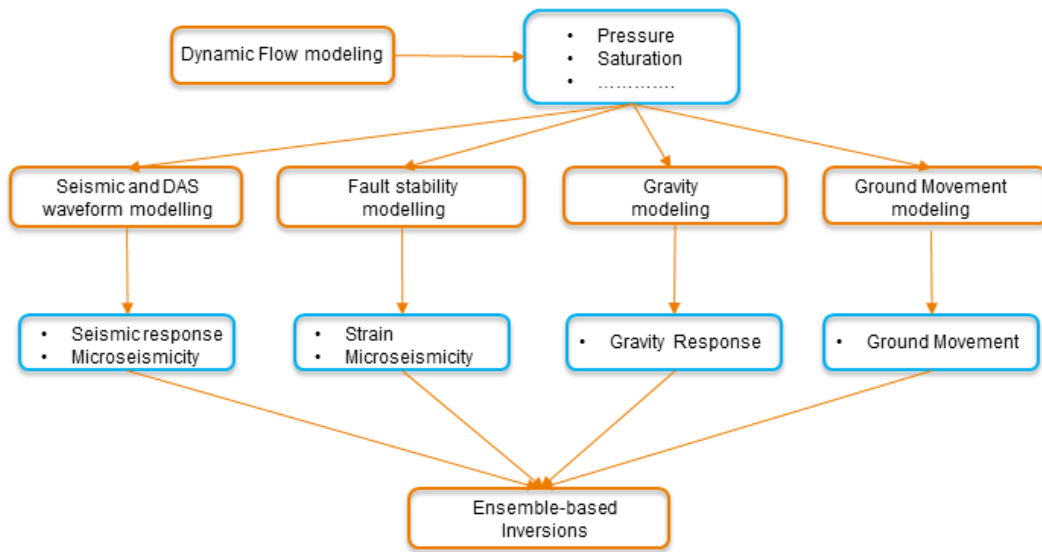


Figure 1. Overview of models set up in task 2.2. Dynamic flow modelling (top left) produces various parameters, like pressure, saturation, etc, which are used as inputs in seismic, geomechanical and gravity models.

2 Approach

We define a modelling framework as a framework of software components that can be used to forward model and simulate processes and situations.

The modelling framework includes seismic, geomechanical modelling and modelling of the gravity response. Monitoring the related geophysical parameters like gravity, seismic velocities, ground movement, etc. is expected to become part of most monitoring strategies (IEAGHG report 2015-02, Xue, 2016, Hannis, 2017, Furre, 2019, IEAGHG report: 2020-01, Furre, 2020). A modelling framework including these parameters, will enable us to simulate various geophysical responses of a CO₂ injection site and will allow us to implement the framework in ensemble-based inversion work (not part of this deliverable) in the future.

There are many options when it comes to software and models to simulate the response of CO₂ injection sites. Already early during the proposal phase of the project, we decided to focus merely on a limited number of processes. The selected physical processes were thought to be relevant, cost-efficient to monitor and were within reach of our combined expertise.

These are:

- Monitoring of the CO₂ plume, and pressure build up using micro gravity and ground movement. The goal is to expand the applicability of monitoring tools (micro gravity and ground movement) for reservoir monitoring. The work is mainly be executed by OCTIO and NORCE.
- CO₂ Saturation using seismic methods. The goal is to validate the applicability of (innovative) seismic methods like DAS (located in wells and /or on the surface) for monitoring the CO₂ saturation in and possibly outside the intended storage reservoir. This work is mainly be performed by NORCE and TNO.
- Fault stability during pressure build up via comparison between modelled strain-induced fault slip and DAS resolution. This holds a direct link to desired (DAS) receiver geometries and their impact on the detection and localization thresholds and magnitude estimation. This work is mainly be executed by TNO.
- Earth model linked to a dynamic flow model(s) and simulations. Although very relevant, we will only briefly describe this, as initial information from these models are taken more or less for granted, and subsequent workflows are aimed to improve the accuracy of these models (e.g. like the ensemble based inversion workflows).

In the coming sections we describe the models separately, even though part of the strength lies in the integration of the models and results.

2.1 Links to other WP's

A lot of seismic modelling work, mostly related to DAS, has already been performed in WP1. Part of this work is described in Deliverable 1.3: DAS synthetic dataset and in Baird *et al.*, 2020 and in Vandeweyer *et al.*, 2021.

In WP1 two popular open source software packages are chosen to model the full seismic response. These packages are SW4 (Sjögreen & Petersson, 2012; Petersson & Sjögreen, 2018) and SPECFEM3D (Komatitsch & Tromp 1999; Tromp *et al.* 2008; Peter *et al.* 2011). Additionally, for simple models analytical and semi analytical approaches are used (e.g. ray-theory and wavenumber integration methods). The knowledge gathered in WP1 has directly been put to use in the activities of Task 2.2, see also Section 3.2 of this document.

The DigiMon monitoring system is developed to have both technical and societal requirements in-mind. A product design process involving (local) stakeholders, using the novel tool of “Societal Embeddedness Level-methodology” (SEL), will ensure that the developed monitoring system will both be technically feasible and fulfill social requirements (WP3). Outcomes of the public awareness work in WP3 were at the time of writing not (yet) available to us. We do know that work is underway, and in the future, these results from public awareness studies will be incorporated in the monitoring strategies (Task 2.4 and 2.6).

3 Modelling Framework

Through monitoring we can address risks and containment at CO₂ storage sites. But taking measurements is merely half the story. To interpret and understand what is actually happening at a storage site, models are needed. These models are necessary to explain and link the measurements to activities, processes and mechanisms. The measurements can be used to improve model parameters and the models can be used to forecast (forward modelling) measurements.

In the next chapter we describe the software components from the modelling framework, and how they can be used to forward model and simulate processes and situations relevant for offshore CO₂ storage.

3.1 Gravity modelling

4D gravity monitoring provides a direct measurement of changes in the mass distribution in the subsurface. Hence, a typical application is monitoring the movement of gas-water contacts exploiting the density contrast between the two fluids. In contrast to other geophysical monitoring techniques, 4D gravity is sensitive to mass changes only and therefore provides a quantitative tool to determine the fluid saturations and densities within the CO₂ plume, and the corresponding fraction of dissolved CO₂ into the brine.

4D micro-gravity as a monitoring technology has evolved since the late '90s and are now routinely being used in most gas fields on the Norwegian Continental Shelf including both the Sleipner and Snøhvit CO₂ storage sites. At Sleipner this method has been used to constrain CO₂ density (Alnes *et al.*, 2008) and the fraction of CO₂ dissolved in brine (Alnes *et al.*, 2011; Chadwick *et al.*, 2005; Hauge *et al.*, 2015). While seismic is effective at delineating the CO₂ plume, 4D gravity data is much better at quantifying the mass changes. Combining seismic and 4D gravity has also shown to increase the combined vertical resolution in the two data types (Landrø and Zumberge, 2016). Here 4D gravity data is used as a complementary source of information on the total mass change within all layers to compensate saturation change suggested by the time-lapse seismic inversion for the seismic shadow effect and the fact that there is a low seismic sensitivity for saturation changes from 0.3 and above.

For relative gravity, the cutting-edge precision in measurements at the seafloor is below one μGal (Ruiz *et al.*, 2020). Depending on the specific field, this corresponds to sub-meter resolution in monitoring movements in the gas-water contact. With this method, a 2D map of 4D gravity changes at the seafloor is generated based on measuring high accuracy relative gravity at specified locations on the seafloor in dedicated surveys. An illustration of the survey technology is provided in Figure 2.

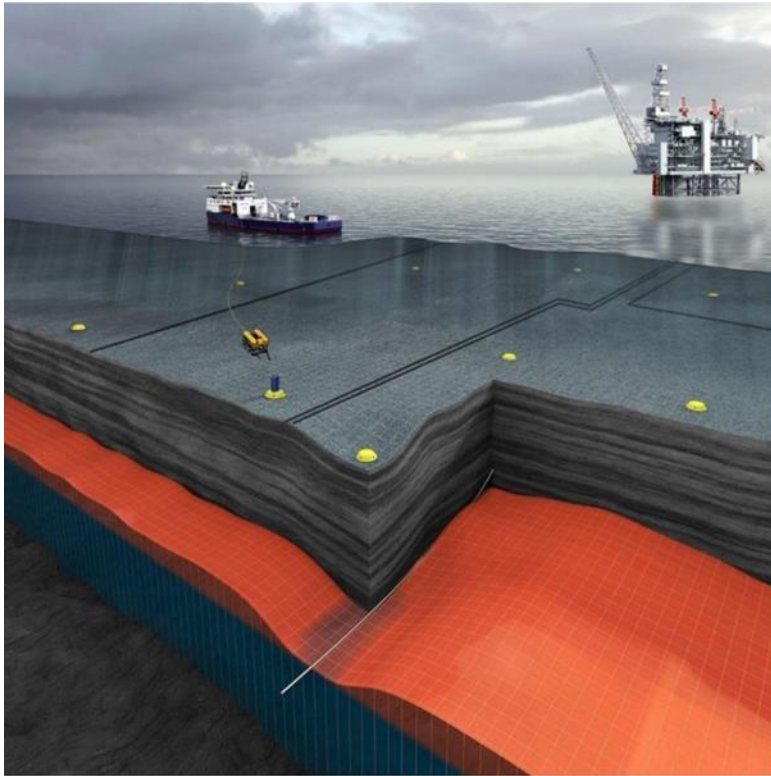


Figure 2: Sketch of the method of deployment of the measuring instruments on the (semi-permanent) concrete stations positioned at the seafloor above the injection site for acquisition of 4D gravity data (Lien *et al.*, 2017)

In Figure 3, is an example showing the 4D gravity signal measured above the Snøhvit and Albatross fields in a 2011-2019 time-lapse sequence taken from Ruiz *et al.*, 2020 . The 2D map of gravity changes at the seafloor provides an image of the mass redistribution in the reservoir. Here a positive signal refers to water influx, and a negative signal refers to gas takeout during production.

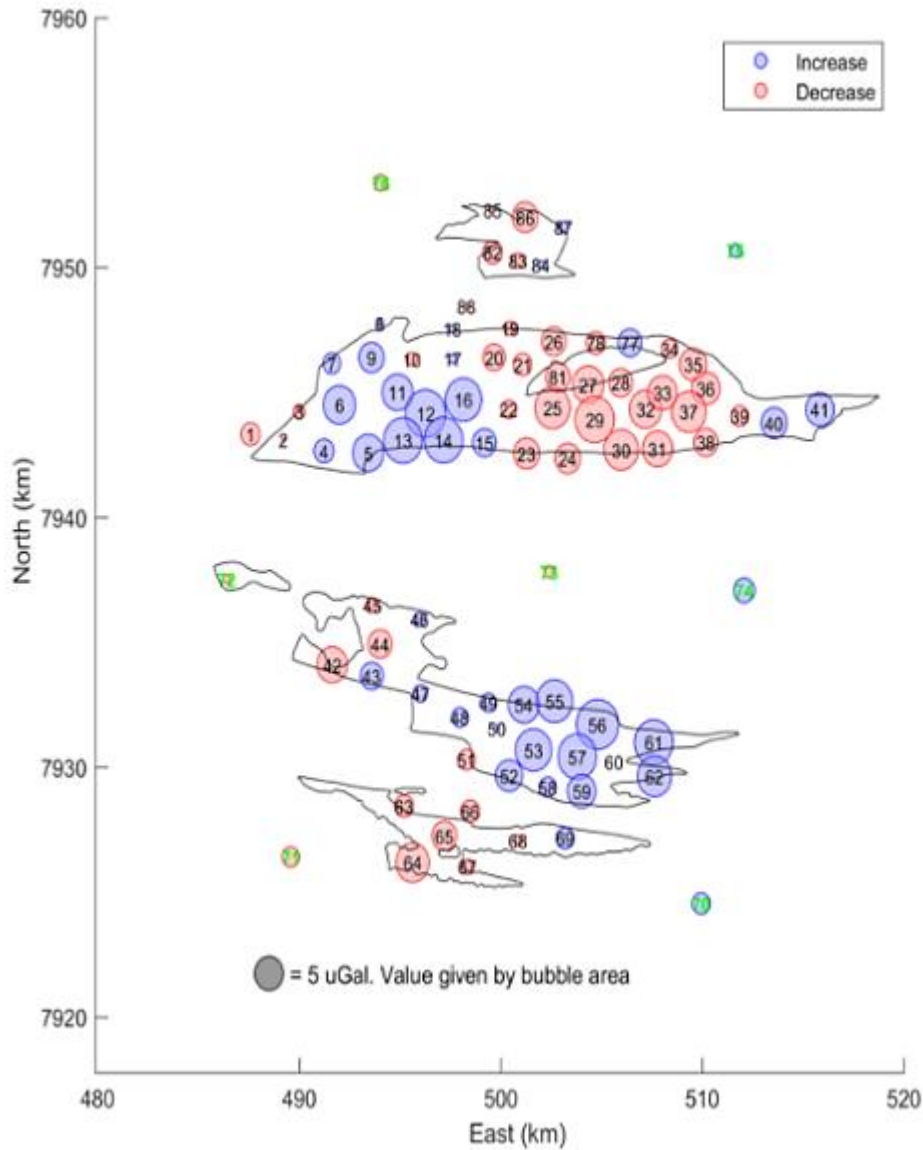


Figure 3: Measured gravity change above the Snøhvit and Albatross fields between 2011 and 2019. The size of the bubble gives the magnitude of the gravity change. Figure taken from Ruiz *et al.*, 2020.

The relation between mass changes in the reservoir and the resulting 4D gravity signal at the seafloor is straightforward to compute from Newton's law of gravity. Given the limited volume of each grid cell relative to the burial depth of the reservoir, the contribution from each grid cell to the gravity response at the seafloor can be computed using the approximation of point masses which gives the following expression for the 4D gravity response at the seafloor:

$$\Delta g = G \sum_i (z_i \Delta m_i) / (x_i^2 + y_i^2 + z_i^2)^{3/2}$$

Here G is the gravitational constant, Δm_i is the mass change between base and repeat surveys within grid cell i , and (x_i, y_i, z_i) is the vector joining the observation point on the seafloor to the center of reservoir cell i . The mass change within each grid cell is a function of changes in fluid saturations, densities, and pore volume, and is given as follows:

$$\Delta m_i = V_i^{t_1} \cdot \sum_{\alpha} \rho_{i,\alpha}^{t_1} \cdot S_{i,\alpha}^{t_1} - V_i^{t_0} \cdot \sum_{\alpha} \rho_{i,\alpha}^{t_0} \cdot S_{i,\alpha}^{t_0}$$

Here V_i denotes the cell pore volume, the superscript t_0 and t_1 refer to the times of the baseline and monitor surveys respectively, and $\rho_{i,\alpha}$ and $S_{i,\alpha}$ denote the density and saturation of phase α (oil, gas and water).

In DigiMon, the forward modelling of the 4D gravity response will be computed using a dedicated 4D - gravity modelling software built on the point-mass approximation as delineated above. This software can be coupled to any forward simulator and takes as input the pore volumes, fluid saturations and densities at different snapshots in time together with the grid geometry of the dynamic flow simulator.

Due to the simplicity of the forward model, the 4D gravity modelling does not impose any constraints on the run-time for the data simulations and facilitates accurate computations of the 3D response utilising the spatial resolution as given by the discretization of the dynamic flow simulator. Moreover, the simple linear relation between gravity measurements and the fluid saturations in the reservoir facilitates an unbiased interpretation of the data.

3.2 Ground movement modelling

Seafloor deformation is an observable effect of reservoir compaction or expansion, caused by pressure depletion, pressure build-up, or temperature changes. Surface deformation monitoring has been a focus of interest in recent years, due to increasing attention on fault activation and induced seismicity (Rutqvist *et al.*, 2016). Experience from the onshore In Salah CO₂ storage project has demonstrated that frequent and high-resolution surface deformation data can contribute to study potential fault reactivation (Ringrose *et al.*, 2013).

Field-wide seafloor deformation monitoring can be provided with millimeter precision by using high accuracy measurements of pressure at the seafloor (Lien *et al.*, 2017; Hatchell *et al.*, 2019). Originally this technology was developed to provide high accuracy depth correction data for 4D micro-gravity monitoring offshore, but it also provides a powerful monitoring tool on its own. In this method, water pressures are measured on top of 20 to 120 semi-permanent concrete stations at the seafloor (see Figure 2 for a conceptual sketch of the survey method), depending on the field size. Stations are located both above and surrounding the field, the later ones being used as a time-lapse reference.

In a subset of the stations, tide gauges are deployed during the whole survey, as a mean for correcting raw pressure measurements for tides and other temporal variations in the water and air column during the survey caused by for example changing weather conditions or current induced density variations in the water column. The amplitude of surface waves with wavelength less than two times the water depth decays exponentially with depth and has minimal effect on seafloor pressures at depths above 80 meter.

The corrected pressure data is then converted into a measurement of relative station depths across the field, which in turn allows monitoring subsidence through the time-lapse changes in relative depths with a precision of a few millimeters.

Figure 4 shows a sample 2D map of seafloor deformation data as acquired above the Snøhvit and Albatross fields in the 2011 -2019 time-lapse (Ruiz *et al.*, 2020). The lateral extent of the signal informs about the pressure depletion pattern, and the magnitude of the deformation together with pressure data from wells inform about the pore compressibility of the reservoirs.

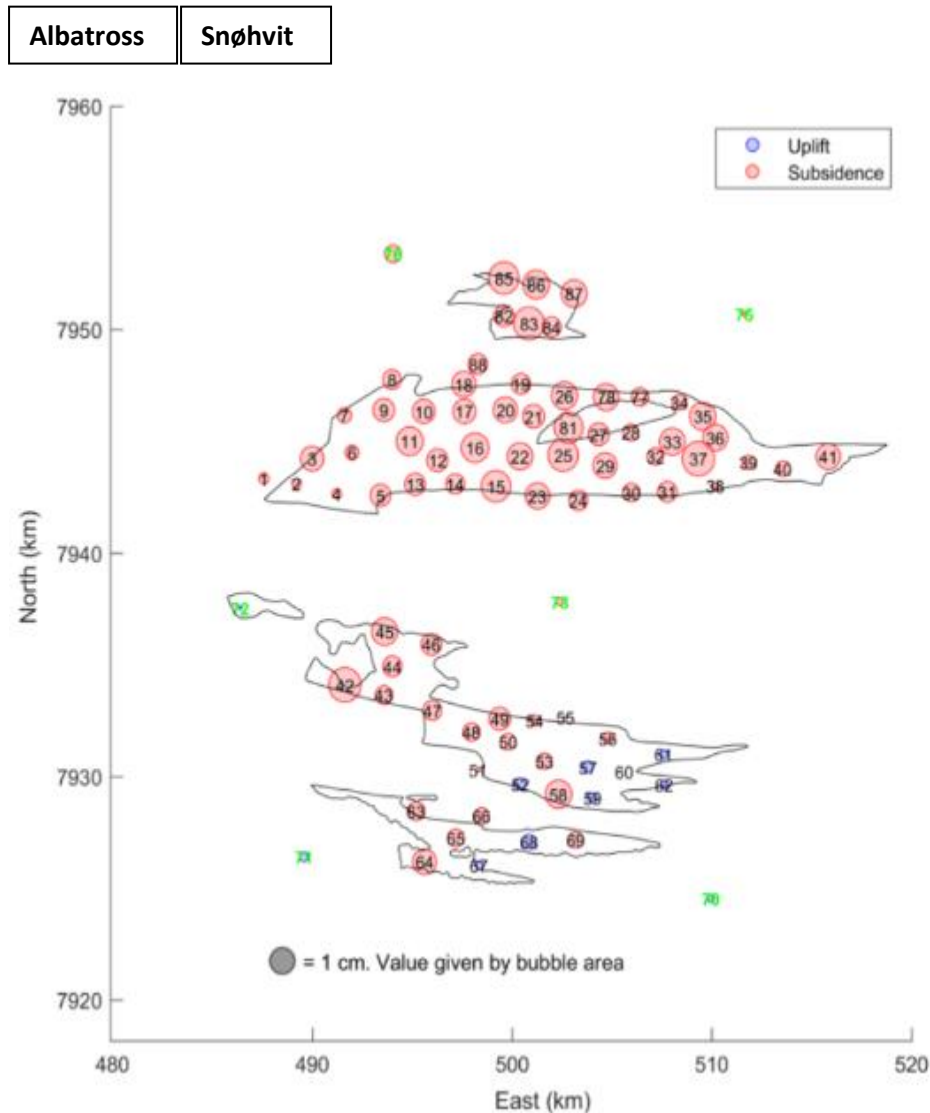


Figure 4: Subsidence measured between 2011 and 2019 measured over the Snøhvit and Albatross field. Each bubble refers to one measurement point at the seafloor. The bubbles denoted in green are placed at a distance from the field where no production induced subsidence or changes in gravity are expected and serves as time-lapse calibration points for the method. The size of the bubble indicates the magnitude of subsidence. Figure taken from Ruiz *et al.*, 2020.

The relation between deformation of the ground surface (as the seafloor) and the reservoir pressure changes can be complex. However, for several field applications, simple semi-analytical modelling tools have proven to be valuable, see for example Alnes *et al.*, 2010, van Thienen-Visser *et al.*, 2015. These semi-

analytical approaches involve multiple forward modelling steps. The first step is to convert the reservoir pressure changes in terms of compaction or expansion. Multiple analytical models for rock compaction based on laboratory measurements and/or field measurements are still highly debated (van Thienen-Visser *et al.*, 2015; Hettema *et al.*, 2002, De Waal, 1986, Spiers *et al.*, 2017, Pijenburg *et al.*, 2018, 2019). A linear elastic compaction model is assumed in DigiMon, with a linear relationship between pressure change Δp_i and pore volume change ΔV_i , such as:

$$\Delta V_i = V_i \Delta p_i C_i,$$

where C_i is the pore compressibility in grid cell no. i in the reservoir; $i = 1, \dots, N_c$ and N_c is the number of active grid cells in reservoir (and aquifers). In practice, the pore volume changes can be outputted directly from Eclipse or re-computed using the C_i outputted from Eclipse.

The second step consists in translating the compaction of each grid cell in terms of seafloor deformation. For this step we make use of transfer functions (also called influence functions or Green's functions), which are rotationally symmetric seafloor displacement profiles for a unit volume of compaction (a nucleus of volumetric strain). These transfer functions honor the mechanical response of the subsurface. We choose to focus on the analytical transfer function T developed by Van Opstal, 1974, which account for the presence of a stiff basement below the reservoir/aquifer system. Combining the Van Opstal's transfer function with the compaction field, the total seafloor deformation S_j can be calculated at the desired observation points, such as:

$$S_j = \sum_i \Delta V_i \cdot T(\bar{r}_{ij}, \nu).$$

$j = 1, \dots, N_{obs}$ and N_{obs} is the number of observation points. The Van Opstal's transfer function is only dependent on the Poisson's ratio ν and the distance \bar{r}_{ij} between the compacting nucleus (i.e. as represented by grid cell no. i) in the reservoir and observation point j . In our approach, seafloor deformation scales linearly with the pressure change in the reservoir during injection $S_j \propto \Delta p_i$ for given C and ν .

3.3 Seismic and DAS modelling

The goal is to develop and describe tools or a workflow to monitor CO₂ saturation in and possibly outside the intended storage reservoir, by making uses of (innovative) seismic methods like DAS (located in wells and /or on the surface).

Using experience and outcomes of tests performed in WP1 we investigated the suitability of seismic simulation packages SW4 and SPECSEM3D, to model the seismic response. From WP1 we learned that SW4 and SPECSEM3D produce comparable modelling results if set up correctly, see D1.3 report and Vandeweyer *et al.*, 2021 and illustrated in

Figure 5.

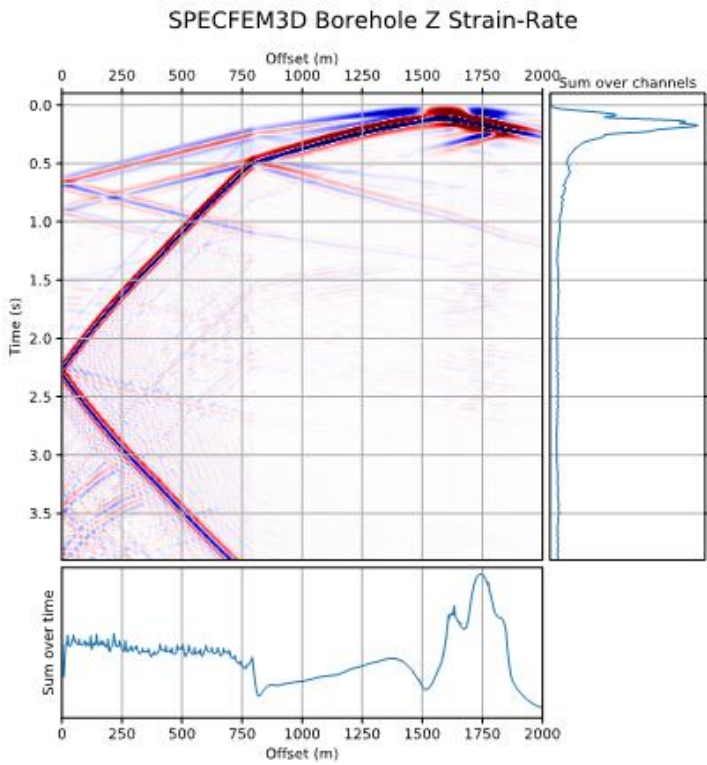
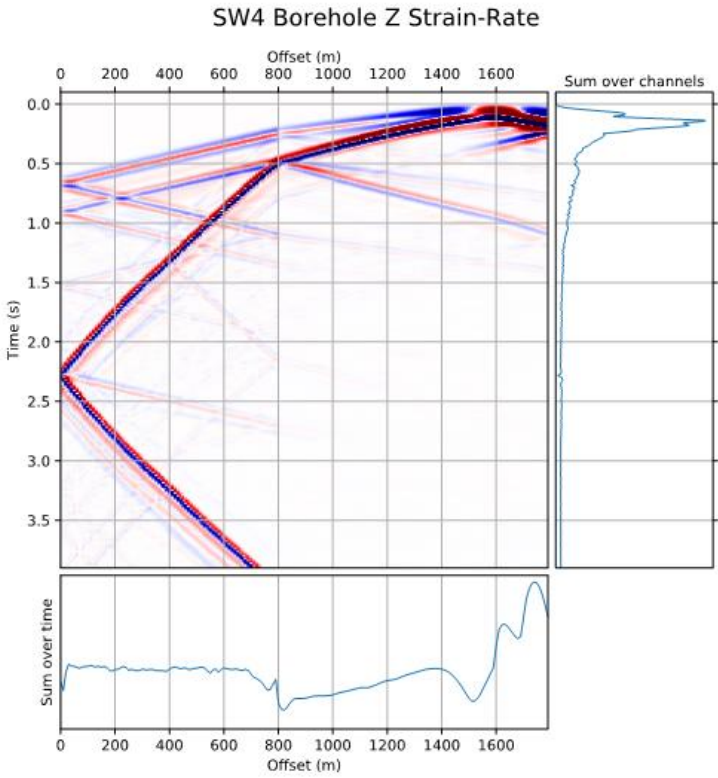


Figure 5. SW4 and SPECFEM3D strain-rate synthetics for a synthetic model recorded along a vertical borehole array. Channel 0 is located at the surface, with the base of the array at 2000 m depth. The source is located at a depth of 1630 m (Vandeweyer, 2021).

We also investigated analytical / raytracer code. These codes can be very fast but cannot simulate the complexity of the complete wave field. These models merely provide arrival times of various waves.

Because of the added complexity of the conversion of a DAS signal to particle velocity (or *vice versa*) we investigated the relevant pros and cons of SW4 and SPECFEM3D, see table 1.

Table 1. Basic pro and cons of SW4 and SPECFEM3D

Software	Pro	Con
SPECFEM3D	<ul style="list-style-type: none"> • SPECFEM3D allows one to put a receiver at any point within the mesh. 	<ul style="list-style-type: none"> • More difficult to get a model geometry up and running. SPECFEM3D requires a quite complicated mesh. • SPECFEM3D can only output particle motion (displacement or velocity).
SW4	<ul style="list-style-type: none"> • Fairly easy to get a simple model geometry up and running. SW4 can use a simple cartesian grid. • SW4 supports the output of all the components of the strain tensor at each station directly" 	<ul style="list-style-type: none"> • SW4 requires receivers to be located at grid nodes.

Internal discussions led to the following conclusions:

1. A DAS system records strain (or strain-rate) and because **SW4 can output strain** seismograms directly, one can convert these strain seismograms to strain-rate very easily by applying an additional time derivative. This post-processing is required to convert SW4 output into DAS synthetics.
2. The **particle motion limitation of SPECFEM3D** is not a major issue for modelling straight fiber cables, as axial strain-rate can be computed in post-processing by computing the spatial gradient of the in-line component of the velocity synthetics using 2nd order accurate central differences with 1m channel spacing. More specifically, the 3rd equation of Wang *et al.* (2018) can be followed. However, if one wants to model the response of more complicated shaped fibers (e.g. helically wound cables) this might quickly become very complicated.
3. Allowing to place **a receiver at any point** within the mesh is particularly important for modelling DAS because it samples the wavefield at very closely spaced channels (~1m spacing). This means that SW4 might require a much higher resolution grid than would otherwise be required to accurately model the wavefield. This would immediately have the undesired effect of increasing calculation times. SPECFEM3D on the other hand enables to place a receiver at any point within the mesh without affecting calculation times.

The fact that SPECFEM3D enables to place a receiver at any points within the mesh without compromising calculation times, is a key element to decide to use SPECFEM3D for our DAS and also conventional seismic modeling work.

3.4 Fault stability modelling

Fault reactivation, potentially induced by the reservoir pressure build-up during CO₂ injection, can be seen as both (1) a threat but also (2) an opportunity to monitor the pressure build-up itself, the fault frictional properties (see Candela *et al.* 2019), and the reservoir elastic properties (see Candela *et al.* 2021).

In DigiMon we focus on making the link between our fault stability modelling and DAS measurements. The objective is to demonstrate that DAS measurements can be used to condition the parameters of fault stability modelling. To reach this objective, the modelling components (Figure 6) are:

1. Simulation of the development of induced stresses at faults during CO₂ injection,
2. Simulation of the slip at faults where the induced stresses reached the frictional strength and faults can potentially start to slip,
3. Simulation of the induced displacements, strains, stresses, due to slip at faults, at any locations of interest (e.g. along well path, at reservoir-caprock interface, at seafloor).



Figure 6. Modelling components of the fault stability modelling.

Our developments are thus targeting both: (1) a better understanding of the threats/risks attached to the reactivation of faults, and (2) the leveraging of the DAS measurements as a mean to calibrate our fault stability modelling approach.

The simulation of the induced stresses at faults due to the reservoir-pressure increase is carried on with MACRIS (**M**echanical **A**nalysis of **C**omplex **R**eservoirs for **I**nduced **S**eismicity, Wees *et al.*, 2019). This software tool has been recently developed by TNO to specifically honor 3D complex reservoir geometries while affording a fast-computational time to be adapted for an inversion scheme. Indeed, MACRIS is a unique technology in the sense that induced stresses at faults can be resolved in 3D with a meter-scale resolution over hundreds of geometrically complex faults. The same spatial resolution could only be obtained for a 2D cross-section of the complex reservoir if a Finite-Element solution would be followed. The disadvantage of MACRIS is that small-scale intra-reservoir elastic heterogeneities cannot be resolved.

The two main geomechanical processes activated during CO₂ injection and honored by MACRIS are:

1. the change in volume of the reservoir, so called poro-elastic effect;
2. the decrease of the effective normal stress at fault due to the increase of the fault pore pressure.

Both geomechanical processes can induce changes in effective stresses in the rock volume which can ultimately lead to the reactivation of pre-existing faults at both levels: the reservoir and its burden.

MACRIS can directly take as input the 3D mesh of complex reservoir flow simulations (e.g. from ECLIPSE, OPM, GEM...). There is thus no need to build a new mesh for the geomechanical modelling as it would be

the case following a Finite-Element package such as Abaqus or Diana. Indeed, each cell of the reservoir flow grid is treated as a nucleus of strain (Mindlin and Cheng, 1950). The inflation of each nucleus of strain (due to the reservoir-pressure increase) can induce stresses at nearby faults; this is the poro-elastic effect. Assuming a-priori scenarios in terms of fault permeability, one can compute the decrease of the effective normal stress at faults from the reservoir pore pressure adjacent to the faults.

Faults where induced stresses exceed the frictional strength can potentially be reactivated and thus slip. The fault slip is modelled assuming an “instantaneous” slip-weakening model (Candela *et al.*, 2019; Wees, 2019). From the slip at faults, and making use of influence functions (e.g. Okada, 1992; Nikkhoo and Walter, 2015), one can derive the induced displacements, strains and stresses in the elastic medium around it. Besides modelling fault reactivation and the potential fault slip attached to it, we are thus also interested in evaluating if this fault slip can be recorded by DAS measurements. The modelled slip-induced strains at specific locations of interests where DAS could be deployed (e.g. along well path, at the seafloor) will be thus compared to the DAS resolution.

The deployed fault stability modelling framework will be applied for both: (1) a synthetic-simplified reservoir field case, and (2) the Smeaheia field case. The magnitude of slip (that is the magnitude of the seismic events) will be conditioned by: (1) the initial stress conditions, (2) the injection scenarios (that is the magnitude of the pressure build-up), and (3) the reservoir geometry (e.g. fault orientation...). The magnitude of the slip-induced strains will be conditioned by the distance between the faults (i.e. the sources) and the receivers-locations of interest. On top of the pre-existing faults of the reservoir flow model, other fault planes will be considered at various distances from receivers-locations of interest. The receivers-locations of interest will correspond e.g. to the well-locations and the caprock/reservoir interface. An ensemble of multiple scenarios should be screened to evaluate what are the specific conditions where the modelled slip-induced strains could be picked-up by DAS.

3.5 Dynamic flow modelling

The dynamic flow modelling is an integral part of both forward and inverse modelling. It provides vital information on flow dynamics and pressure distributions of the subsurface over times. The modelling is usually executed by using reservoir simulation models. The main idea is to solve the partial differential equations that describes the fluid-flow on numerical grids (Aziz, K., Settari, A, 1979). In most cases, the unknowns are the various saturation phases (oil, water, gas) and pressure values in the grid cells of the model. In the petroleum industry, various types of dynamic flow or reservoir simulators are considered depending upon the needs. For an example, by using a “black oil” simulator the interaction between the oil, gas and water phase can be modelled numerically while keeping the mass balance preserved. More advanced and complex dynamic flow modelling is also available, for instance compositional simulators, models including geo-mechanical effects etc.

For the simulations planned we have chosen to use the Eclipse simulator from Schlumberger. Main reasons for this is that the simulator is relatively fast and accurate. Eclipse is a well-known and broadly implemented simulator all across the petroleum industry, academia and even regulatory authorities. Further to that, the provided reservoir model of the Smeaheia field is in an Eclipse native format.

Figure 7 shows the modelled distribution of CO₂ through years of CO₂ injection for the Johansen benchmark model (Eigestad *et al.*, 2009). This synthetic reservoir model is developed based on the Johansen formation, located below the Troll field. The Johansen benchmark case as described in Eigestad *et al.*, 2009, is publicly available. The reservoir model consists in total of 11 layers and is divided into three geological zones. The Johansen Formation forms the main reservoir zones (layers 6-10); and is embedded by the Dunlin shale layers (layers 1-5) above and one shale layer below (layer 11). The model consists of a total of 100x100x11(=110000) grid blocks, of which 88775 are active. The isothermal simulation is run with Eclipse for a total of 150 years where first 75 years being CO₂ injection periods. Here, Eclipse is considered as a preferred simulator for the preliminary study, because it is a fast, robust commercial tool and further is an industry standard. However, other more dedicated tools can also be used for detailed study, for example CO₂ module (MRST-co2lab) of the Matlab Reservoir Simulation toolbox (Lie, 2019).

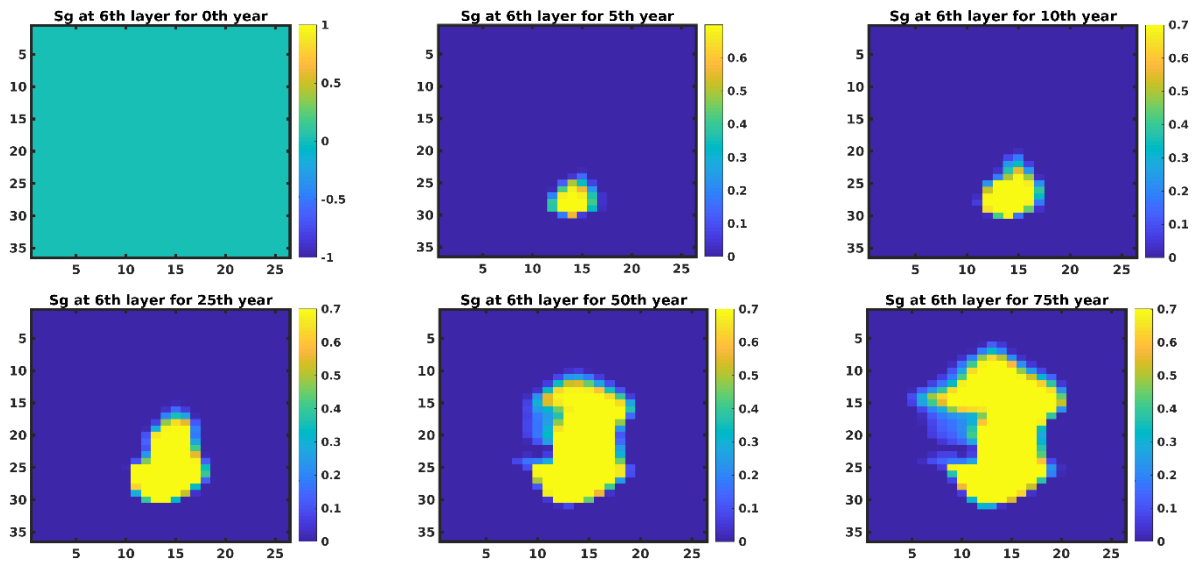


Figure 7. Movement of CO₂ at layer 6 of the Johansen benchmark model. Here, only part of the layer (35x25) is shown.

4 Towards field cases

For WP2 we decided to base our modelling work around the Smeaheia structure, Figure 8. It is our intention to use unified input data (as much as possible), to be able to compare various results as much as possible.

The Smeaheia site is identified as a potential site for large scale CO₂ storage, even though the field development is still immature and more research is required to reduce the model uncertainties.

A main question is whether the pressure depletion due to gas production in Troll (Smeaheia is hydraulically connected to Troll) will reduce the storage capacity of the Smeaheia formation below what is required for large scale storage. The pressure communication with Troll may introduce a pressure gradient in the Smeaheia formation and thereby a preferential flow pattern. Pressure depletion may also lead to reduction in the density of the CO₂ and thereby the storage capacity of the Smeaheia site.

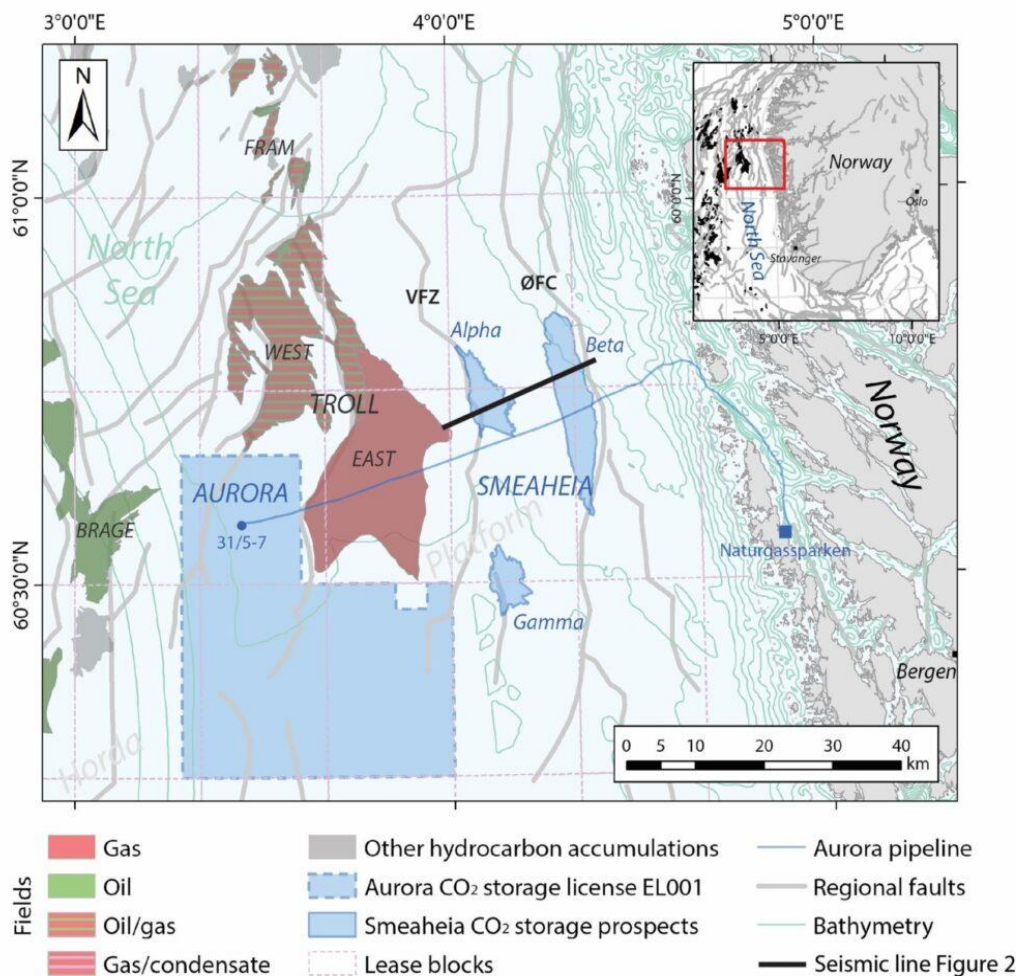


Figure 8. The Smeaheia fault block is bound by the Vette Fault Zone (VFZ) and the Øygarden Fault Complex (ØFC) (Mulrooney, 2020).

When the initial work started in DigiMon, we did not have access to any data or models from Smeaheia. To use our time efficiently we used other, freely available datasets to work with and test our workflows on. For an example, the synthetic Johansen benchmark model (Eigestad *et al.*, 2009) is used to investigate seismic and gravity responses.

Around the end of 2020 Equinor, on behalf of the Northern Lights consortium provided the DigiMon partners access a Smeaheia data package with subsurface data. Amongst this data are two reservoir models, well logs, seismic data, various reports, a Petrel project of Smeaheia, etc.

The Smeaheia site has a fairly homogeneous overburden (no interbedded permeable layers). In the Gassnova founded project (Thiem *et al.*, 2019, CLIMIT Project 616212; Cost-effective microseismic monitoring and processing solutions, OCTIO AS) a feasibility study for using permanent seismic monitoring to detect micro seismic events during injection was done on the Smeaheia model including seismic from 2012. Hence, a velocity model for both V_p and V_s in the reservoir and overburden was set up which is also made available to the DIGIMON project.

The following describes parts of our initial work not necessarily directly linked to Smeaheia, but relevant enough to learn and draw conclusions from.

4.1 Gravity and ground movement modelling

For the initial phase of the work and utilising a publicly available geological model of the area (Eigestad *et al.*, 2009), both gravity and ground movement modelling have been carried out on the Johansen field benchmark case (see Section 3.5) located below the Troll field. Note that the Johansen formation is the selected injection site for the Northern Light project (<https://northernlightsccs.com/>) after the successful drilling of the Aurora well in November 2019.

For the forward modelling of the gravity response a dedicated 4D gravity modelling tool based on point-mass approximation (see Section 3.1) is considered. The tool uses the output of a dynamic flow simulator (such as pore volumes, fluid saturation and densities at grid cells) from baseline and monitor scenarios to simulate the 4D gravity response at a 2D seafloor array of measurement locations covering the injection site. The Johansen formation, which is the formation which receives the CO_2 , is in a varying depth between 2200 m and 3100 m below sea level and the formation thickness ranges from 80 m to 120 m. The average water depth is around 300 m. Figure 9 shows the 4D gravity response for the Johansen case. The base and monitoring scenarios are 0 and 75 years of gas injections, respectively, in this case.

To model seafloor deformation using the van Opstal model (see Section 3.2) the required input parameters are the pore volume change at each grid cell together with the Poisson's ratio of the overburden and coordinates of the simulation grid. Alternatively, also as outlined in Section 3.2, the modelling of reservoir volume changes (compaction/expansion) and the corresponding seafloor deformation can be based on reservoir pressures at selected time stamps and the pore compressibility of the dynamic reservoir model. Figure 10 shows the seafloor deformation due CO_2 for the Johansen benchmark case.

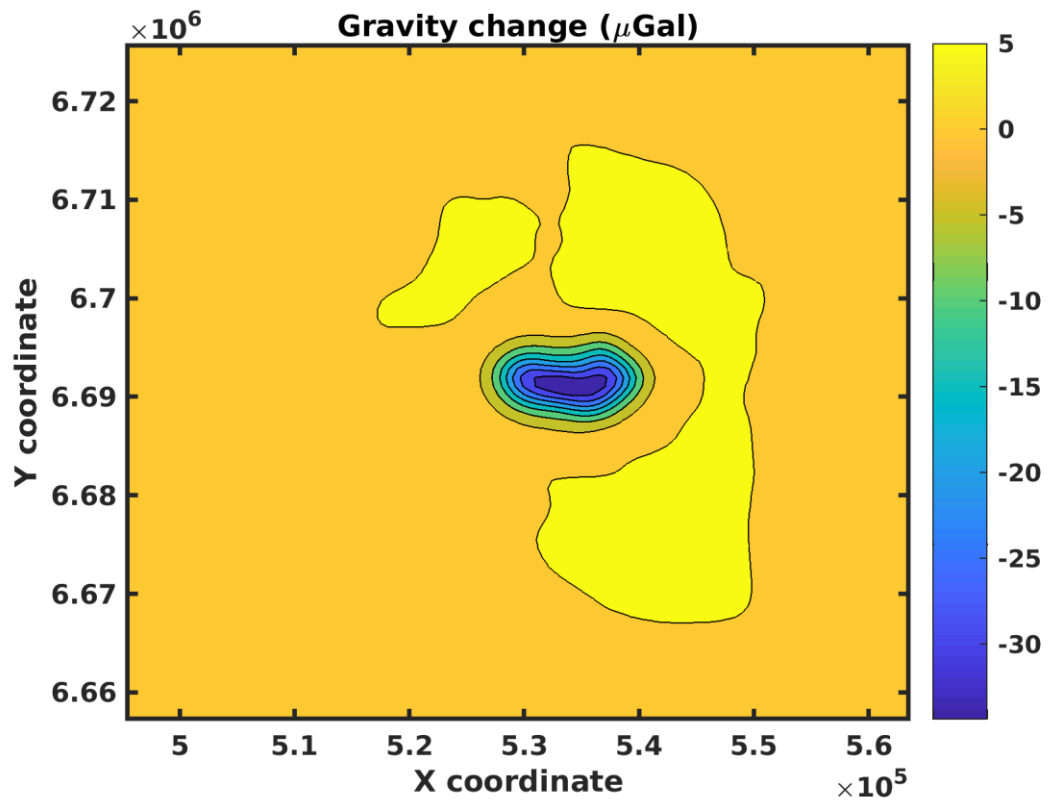


Figure 9. 4D gravity response at seafloor in μGal . Here, monitor and base are 75 years apart. Here, the Johansen benchmark case is considered for the test. A negative 4D gravity signal refers to lighter CO_2 replacing denser aquifer brine.

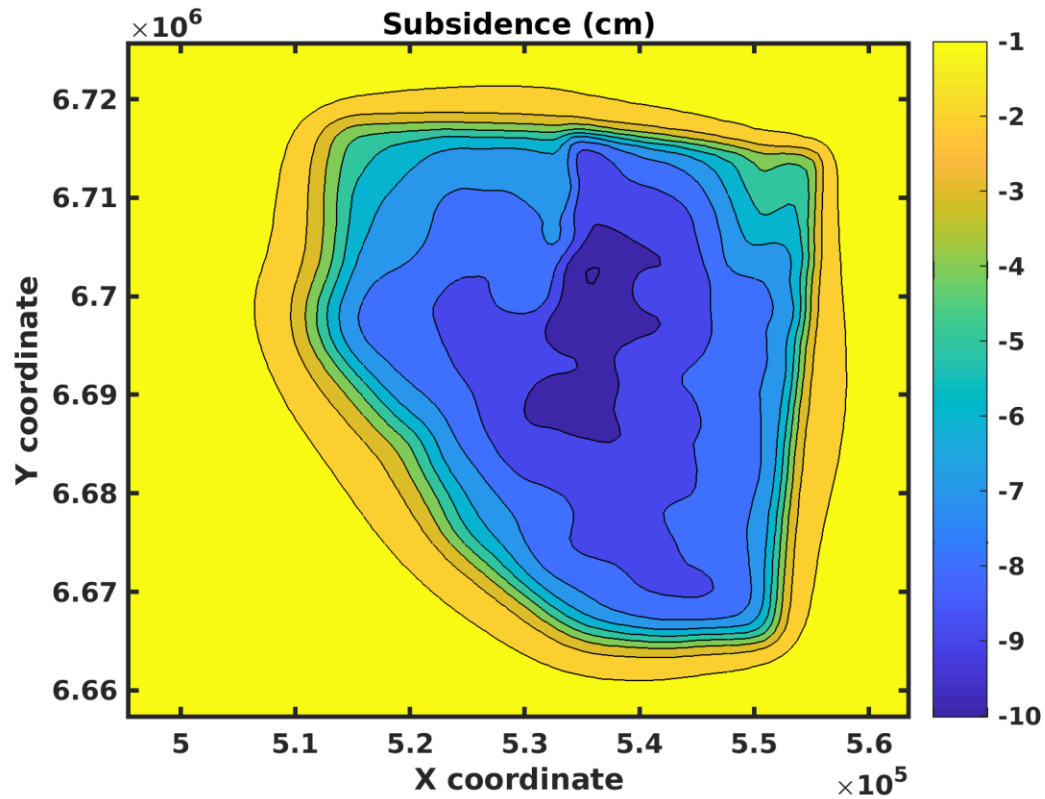


Figure 10. Seafloor uplift in cm after 75 years of CO₂ injection for the Johansen benchmark case. Negative subsidence correspond to seafloor uplift caused by reservoir expansion following the pressure build-up during injection.

We have started investigating the Smeaheia reservoir models, as supplied to us. The results of seafloor deformation for one of the models is shown in Figure 11. The 2D map of seafloor deformation provides a measure of the distribution of the pressure build-up during injection for a period of 80 years. Once the stiffness of the structure is properly constrained (through inverse modelling combining pressure data from wells and the seafloor subsidence data) the magnitude and pattern of the seafloor deformation can be used to delineate and quantify the pressure response of the reservoir. With this approach a sensitivity analysis can be performed exploring the seafloor response for different realizations of either the pressure plume or the stiffness of the reservoir rocks.

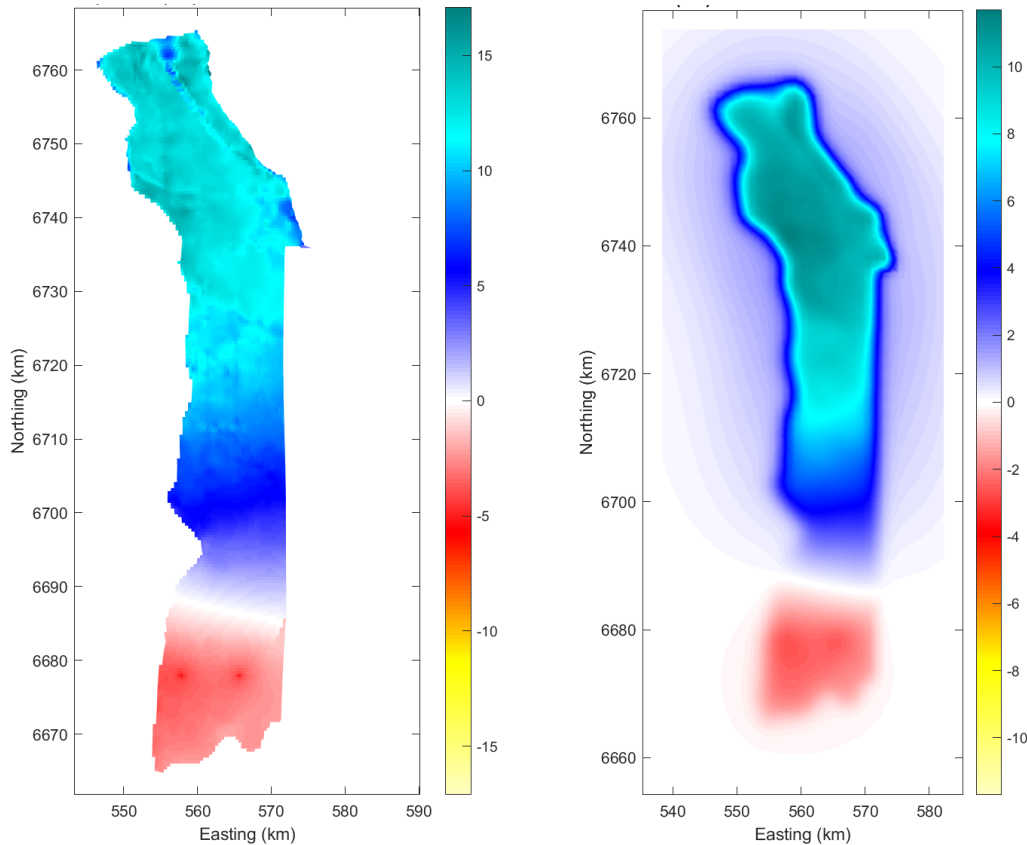


Figure 11. Reservoir compaction in cm (left) and seafloor deformation in cm (right) during CO₂ injection into the Smeaheia site in the time-lapse between January 2021 and January 2102. Here negative values correspond to pore volume expansion and seafloor uplift respectively. The scale of the changes is given by the colour bars in cm's.

4.2 Seismic and DAS modelling

Initial model runs with SPEC3D were done for the Johansen benchmark. The initial runs raised concerns about the computation time of the SPEC3D model. A large number of model realizations are needed in the inversion workflow of task 2.4 - "Integrated interpretation and uncertainty quantification", where both source locations and velocity models are varied in different realizations. Calculation times could not become too large (e.g. preferably less than 30minutes per simulation). For task 2.6 - "Optimize the monitoring solution" probably the same limitations will apply.

A single run in SPEC3D for the central region of the Johansen model, corresponding to an area of 3.0x1.5x2.5 km (Figure 12), already took 3.5 hours (using readily available computational hardware). Further improving the model by including better boundary conditions to suppress site reflections and by including a water layer to mimic offshore conditions even further increased computation times. The same would be the case for SW4, having a comparable demand as SPEC3D on computation time.

To facilitate the large number of model simulations as required in tasks 2.4 - "Integrated interpretation and uncertainty quantification" and task 2.6 - "Optimize the monitoring solution", the "simpler" but faster 2D version of SPECSEM (i.e. SPECSEM2D) was tested and compared against SPECSEM3D. The key difference between the two SPECSEM versions basically is the omission of the third spatial dimension in SPECSEM2D. This is well suited for our application where for now we are mainly interested in source-receiver configuration present inside the same plane. However, the 3D version of SPECSEM should be used, for instance when interested in more advanced source-receiver layouts (e.g. multiple parallel receiver lines) or when considering out of plane reflections.

Figure 13 shows the resulting seismograms for a borehole array computed by SPECSEM3D and SPECSEM2D. Since the modelling results of the two SPECSEM versions were very comparable to each other, the SPECSEM2D package was chosen to be used in the modelling framework, thereby decreasing simulation time to an acceptable 5 minutes per model run, when running the model on (a reasonable) 36 compute cores. For the case when modelling the response of a DAS cable deployed on or just below the seabed, a similar agreement between SPECSEM3D and SPECSEM2D waveform results can be expected, since the numerical implementation of wave equations and boundary conditions for acoustic and elastic media is identical in the two SPECSEM versions.

In addition, we assess whether the effect of any injected CO₂ in the Johansen field would cause significant changes in any seismic recordings. This was done by relating varying stages of CO₂ injection and associated pressure and saturation in to corresponding seismic velocity models based on rock-physics relationships. Figure 14 shows synthetic borehole receivers for velocity models corresponding to 5 and 10 years of storage, with an injection rate of $1.4 \cdot 10^4$ m³/day at reservoir conditions. The difference between the recordings (right panel) clearly shows the effect of the changed velocity model on strength of seismic phases reflected from the reservoir. Figure 15 shows an example of a SPECSEM2D simulation for the Johansen field where the source is placed inside a water column and dense horizontal and vertical receiver arrays are defined to mimic the DAS response. Both the receiver lay-out and source parameterization can be flexibly adjusted. Multiple simulations can be automatically conducted in a sequential way using batch jobs, for instance to generate exploration style reflection data for different shot locations (see Figure 16).

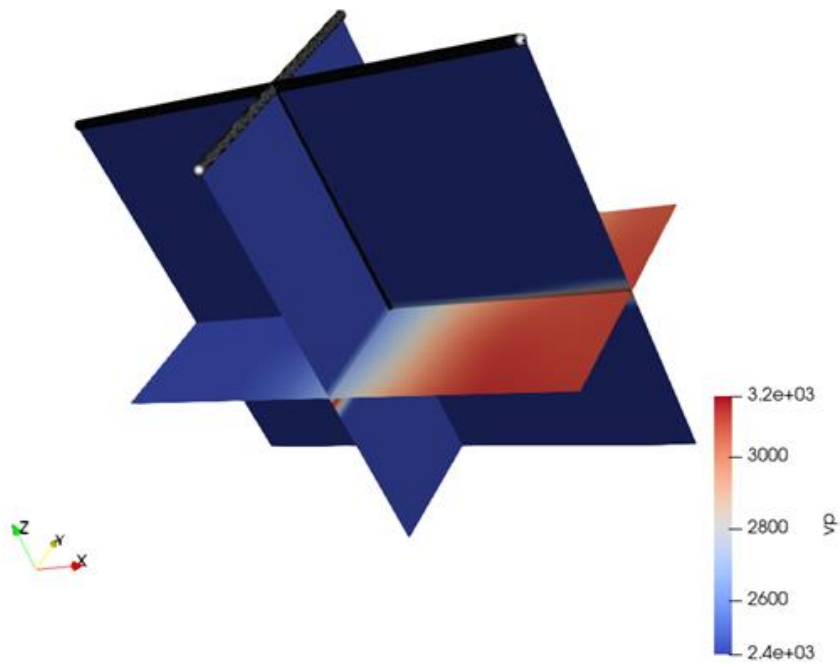


Figure 12. P-wave velocity model used for SPECFEM of the Johansen field.

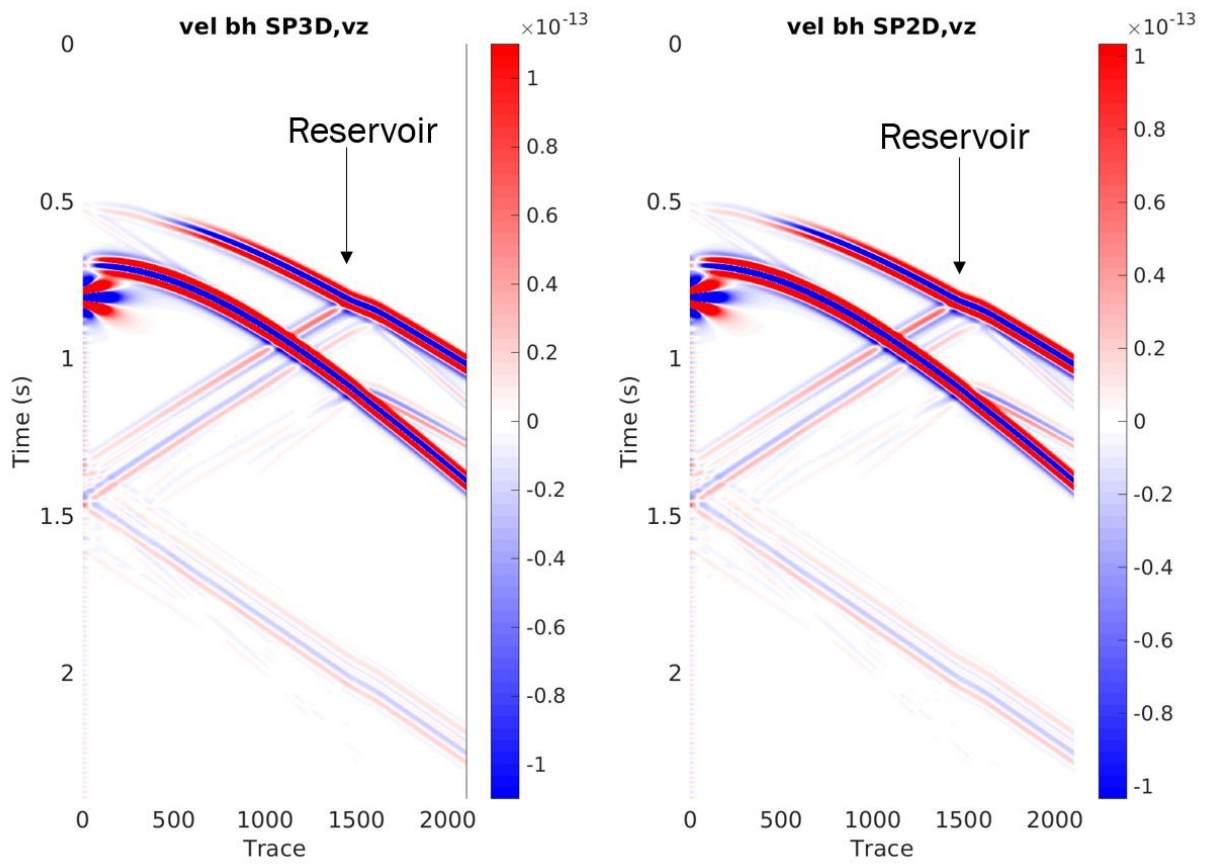


Figure 13. Left: SPEC-FEM3D result of vertical velocity component for a borehole receiver line. Note that depth increases with trace number and the trace spacing is 1 m. Right: SPEC-FEM2D result of vertical component for a borehole receiver line with an identical velocity model and source location as SPEC-FEM3D model.

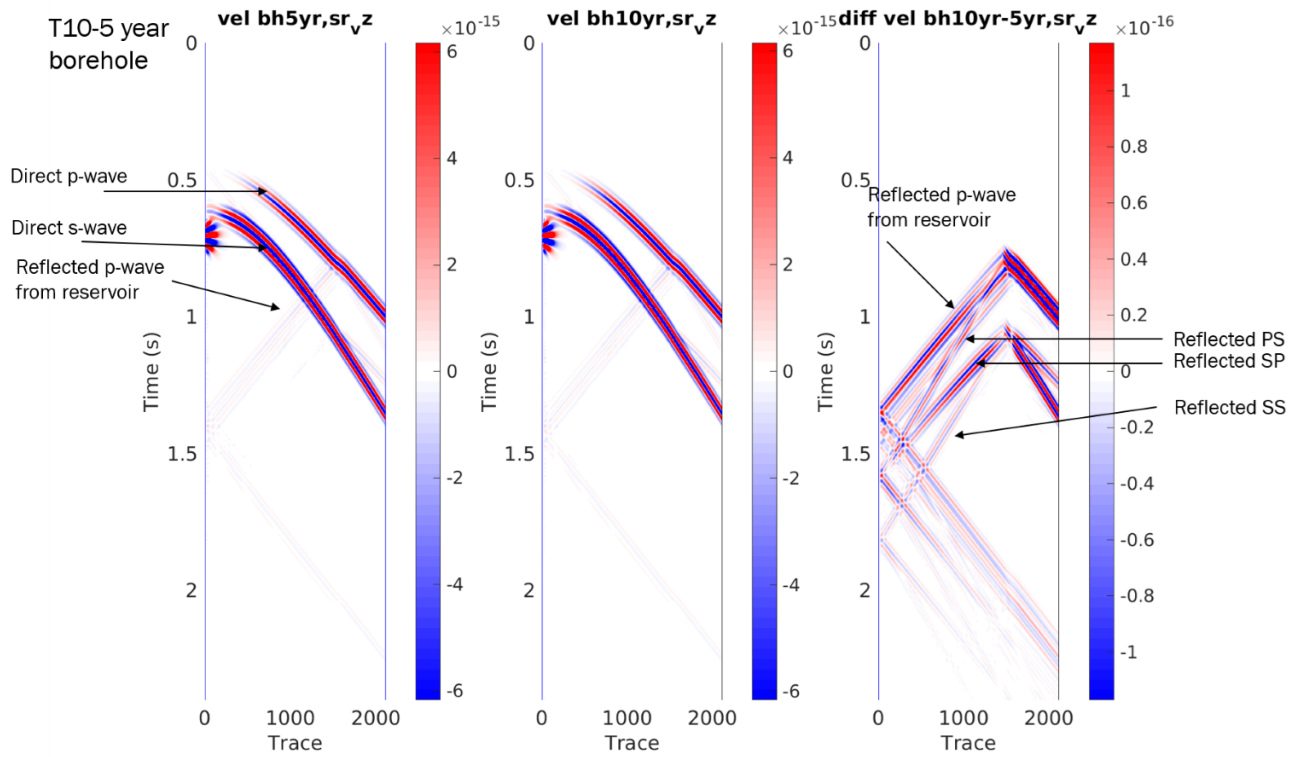


Figure 14. Borehole recordings (vertical strain rate) based on SPECSEM3D simulation for Johansen model after 5 year (left) and 10 years (centre) of CO₂ storage. The difference between the two vintages (right) clearly shows changes in reflection strengths at reservoir level for different seismic phases as indicated in the figure.

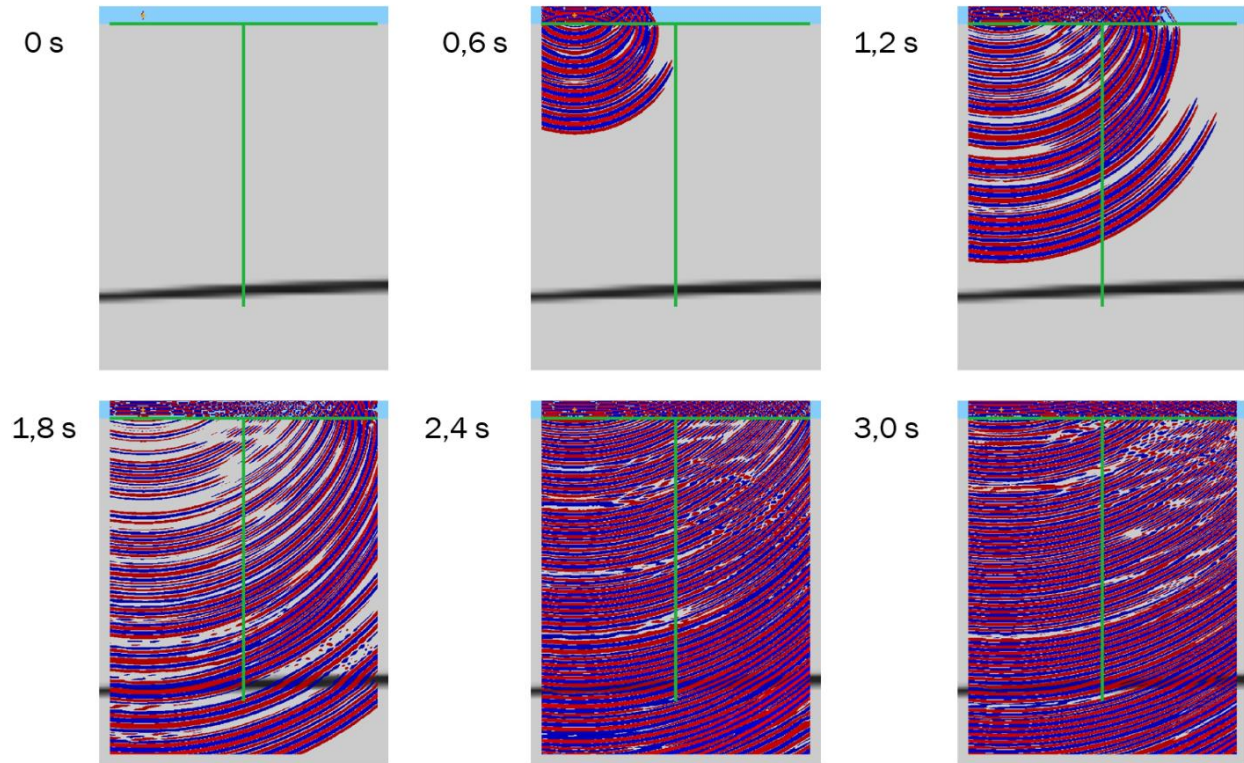


Figure 15. Snapshots of the evolution of wavefield propagation in SPEC2D, for an acoustic-elastic model where the source is positioned inside the water column

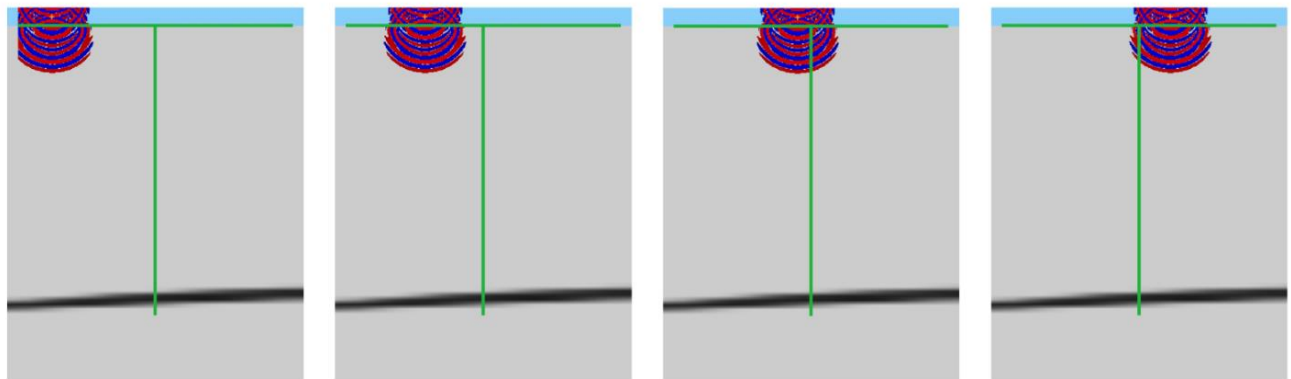


Figure 16. Example of moving source to generate exploration style synthetic DAS reflection data.

The seismic modelling approach of the modelling framework will in the future be tailored to the Smeaheia site and be used for the ensemble based inversion work in task 2.4, to calculate different scenarios for different reservoir injection stages (and corresponding elastic models) as well different source positions. To address the effect of noise within the uncertainty analysis of task 2.6 varying degrees of noise can be imposed to the synthetic seismic data.

Post-processing

Once the SPECFEM2D simulations are completed the raw synthetic data requires some basic processing. This consists of applying a low-pass filter to compute particle velocities and to remove any artificial high frequency noise, followed by the translation of particle velocity into strain rate (as output by DAS) in the direction of the fiber-optic cable. These strain-rate measurements thus are single-component measurements. During the ensemble-based inversion work in task 2.4, synthetic recordings will be inverted towards pressure and saturation. Comparisons can be made between spatially dense single-component strain-rate measurements (DAS equivalent) and spatially coarse multi-component particle velocity (geophone equivalent) to address the added value of DAS measurements.

In addition, the synthetic data can be perturbed with varying degrees of noise levels to accommodate the effect of noise within the uncertainty analysis planned in task 2.6. For this purpose, noise levels are planned to derive from DAS and geophone datasets that are currently at the disposal of the DIGIMON partners.

4.3. Fault stability modelling

The fault stability modelling will be applied on both (1) synthetic single-faulted reservoir model and (2) the Smeaheia field. As explained in section 3.4., the first step of the fault stability modelling consists in computing the development of induced stresses at faults during CO₂ injection. For the assessment of the potential of fault reactivation, the important stress metric to be considered is the changes in Coulomb stress which includes both changes in shear stress and changes in effective normal stresses. Figure 17 illustrates the Coulomb stress changes due to the reservoir pressure changes computed with MACRIS (see section 3.4) for the Norne field. One can expect in a close future similar output for the Smeaheia field.

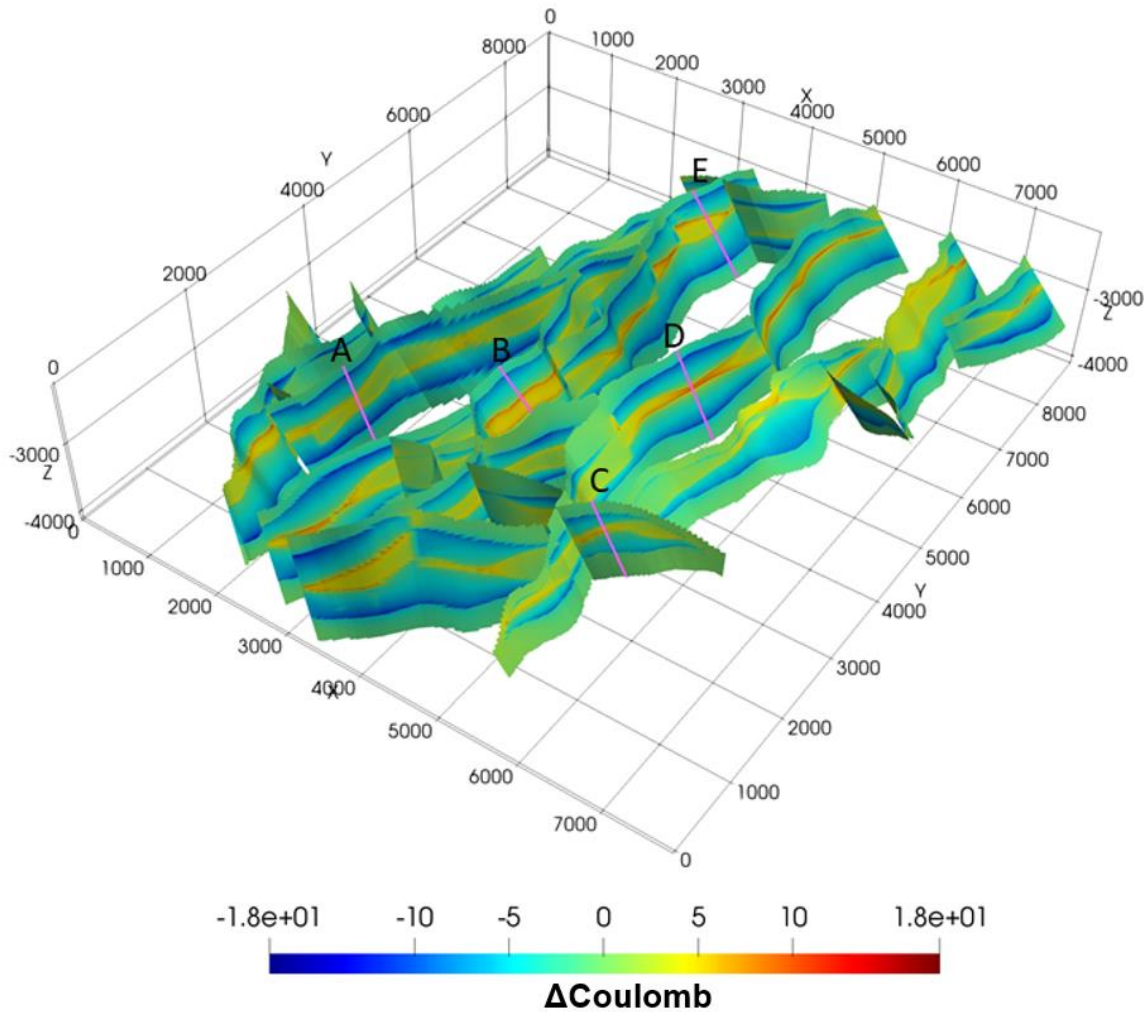


Figure 17. Coulomb stress changes computed with MACRIS for the Norne field (modified from Wees *et al.*, 2019, note the A-B-C-D lines corresponds to other figures not referred to here).

Once Coulomb stress changes will be computed for the Smeaheia field with MACRIS. The next step will consist in selecting a fault of interest where the likelihood of fault reactivation is high, that is where the cumulative Coulomb stresses significantly exceeded the failure line. Then the fault slip post-reactivation will be computed and subsequently the slip-induced strains modelled at locations of interests (e.g. along well path, at reservoir-caprock interface, at seafloor).

5 Conclusions

The DigiMon monitoring system will be developed having both technical and societal requirements in mind.

Over the last few months, we have designed and partially already adapted the modelling framework we set out to create. The technical ways to do so seem endless, but in reality there are many constraints. Focusing on what should be relevant and what is achievable, we created a modelling framework which contains the modelling of

- The gravity response
- The ground motion
- The seismic response
- The fault stability and related seismicity

These models should enable us to monitor:

- The CO₂ plume, using micro gravity:
4D gravity provides a direct measurement of changes in the mass distribution during injection or production. Hence, gives a quantitative measure of the saturation and density distribution of the injected CO₂
- The CO₂ plume, and pressure build up using ground movement:
Seafloor deformation is an observable effect of reservoir expansion and compaction, caused by pressure changes due to CO₂ injection. These pressure changes can be caused by fluid migration, fluid phase transitions, temperature changes and even chemical reactions. For DigiMon we focus on seafloor deformation induced by pressure changes caused by fluid migration and transitions in fluid phase.
- CO₂ saturation using seismic methods:
Saturated and pressurised rocks have different seismic properties. The developed workflow enables us to assess CO₂ saturation in and possibly outside the storage reservoir, by making uses of seismic methods including DAS, located in wells and /or on the surface.
- Fault stability via modelled strain-induced fault slip and seismicity:
Fault reactivation, potentially induced by the reservoir pressure build-up during CO₂ injection, enables us to monitor: (i) the pressure build-up, (ii) the reservoir elastic properties, (iii) and the fault frictional properties.

6 References

Alnes H., Stenvold T., Eiken o., 2010, Experiences on Seafloor Gravimetric and Subsidence Monitoring Above Producing Reservoirs, Conference Proceedings, 72nd EAGE Conference and Exhibition incorporating SPE EUROPEC 2010, Jun 2010, cp-161-00371

Alnes, H. *et al.*, Monitoring gas production and CO₂ injection at the Sleipner field using time-lapse gravimetry, *Geophysics*, 73, 155-161, 2008

Alnes, H. *et al.*, Results from Sleipner gravity monitoring: updated density and temperature distribution of the CO₂ plume, *Energy Procedia* 4, 2011

Aziz, K., Settari, A., *Petroleum Reservoir Simulation*. Elsevier Applied Science, New York, 1979.

Baird A., 2020, Modelling the Response of Helically Wound DAS Cables to Microseismic Arrivals, Conference Proceedings, First EAGE Workshop on Fibre Optic Sensing, Mar 2020, Volume 2020, p.1 – 5

Candela, T., Osinga, S., Ampuero, J.-P., Wassing, B., Pluymaekers, M., Fokker, P. A., *et al.* 2019. Depletion-induced seismicity at the Groningen gas field: Coulomb rate-and-state models including differential compaction effect. *Journal of Geophysical Research: Solid Earth*, 124, 7081– 7104.

Candela T., Peters E, Van Wees J., Fokker P., Wassing B., Ampuero J-P., 2019 Effect of fault roughness on injection-induced seismicity - 53rd US Rock Mechanics/Geomechanics Symposium.

Candela, T., Pluymaekers, M., Ampuero, J.P., van Wees, J.D., Buijze, L., Wassing, B., Osinga, S., Grobbe, N., Muntendam-Bos, A.G. (2021). Controls on the spatio-temporal patterns of induced seismicity in Groningen constrained by physics-based modeling with Ensemble-Smoother data assimilation. in review at *Geophysical Journal International*.

Chadwick R.A., Arts R., Eiken O., 2005, 4D seismic quantification of a growing CO₂ plume at Sleipner, North Sea, Geological Society, London, *Petroleum Geology Conference series*, 6, 1385-1399

Eigestad, G.T., Dahle, H.K., Hellevang, B., Riis, F., Johansen, W.T., Øian, E., 2009. Geological modeling and simulation of CO₂ injection in the Johansen formation. *Comput. Geosci.* 13 (4), 435.

Furre, A.-K., Meneguolo, R., Ringrose, P., Kassold, S.. 2019. Building confidence in CCS: From Sleipner to the Northern Lights Project. *First Break*. 37. 81-87. 10.3997/1365-2397.n0038.

Furre A-K.i, Meneguolo R, Pinturier L, Bakke K, 2020, Planning deep subsurface CO₂ storage monitoring for the Norwegian full-scale CCS project, *First Break*, Volume 38, Issue 10, Oct 2020, p. 55 - 60

Hannis S., Chadwick A., Connelly D., Blackford J., Leighton T., Jones D., White J., White P., Wright I., Widdicomb S., Craig J., Dixon T., 2017, Review of Offshore CO₂ Storage Monitoring: Operational and Research Experiences of Meeting Regulatory and Technical Requirements, *Energy Procedia*, Volume 114, 2017, Pages 5967-5980, ISSN 1876-6102,

Hatchell *et al.*, 2019. Precise depth and subsidence measurements during deepwater OBN surveys - SEG International Exposition and 89th Annual Meeting

Hauge V.L., Kolbjørnsen O., 2015, Bayesian inversion of gravimetric data and assessment of CO₂ dissolution in the Utsira Formation, Interpretation, vol. 3, no. 2, pp. SP1-SP10.

Hettema, M., Papamichos, E., & Schutjens, P. M. T. M. (2002). Subsidence delay: field observations and analysis. Oil & Gas Science and Technology, 57(5), 443-458.

IEAGHG, "Review of Offshore Monitoring for CCS Projects", 2015-02. July, 2015

IEAGHG, "Monitoring and Modelling of CO₂ Storage: The Potential for Improving the Cost-Benefit Ratio of Reducing Risk", 2020-01, February, 2020.

Komatitsch D., and Tromp J., 1999, Introduction to the spectral element method for three-dimensional seismic wave propagation. Geophysical journal international 139, 3 (1999), 806–822.

Landrø M., Zumberge M., 2016, Estimating saturation and density changes caused by CO₂ injection at Sleipner — Using time-lapse seismic amplitude-variation-with-offset and time-lapse gravity, SEG Interpretation, Volume 5, Issue 2, May 2017, Pages: 1M-T277

Lien M., Agersborg R., Hille L.T., Lindgård J.E., Ruiz H., Vatselle M., 2017, How 4D Gravity and Subsidence Monitoring Provide Improved Decision Making at a Lower Cost, First EAGE Workshop on Practical Reservoir Monitoring

Lie, K.A., 2019. An Introduction to Reservoir Simulation Using MATLAB/GNU Octave. Cambridge University Press.

Mindlin, R. D., & Cheng, D. H. (1950). Nuclei of strain in the semi-infinite solid. Journal of Applied Physics, 21(9), 926-930.

Nikkhoo, M., Walter, T. R. Triangular dislocation: an analytical, artefact-free solution. - Geophysical Journal International, (2015). 201 (2), 1117-1139. doi:10.1093/gji/ggv035.

Mulrooney M., 2020, DERISKING THE SMEAHEIA FAULT BLOCK: GEOLOGICAL CONTROLS ON CO₂ CONTAINMENT, [https://blog.sintef.com/sintefenergy/ccs/derisking-the-smeaheia-fault-block-geological-controls-on-CO₂-containment/](https://blog.sintef.com/sintefenergy/ccs/derisking-the-smeaheia-fault-block-geological-controls-on-CO2-containment/)

Okada, Y., 1992. Internal deformation due to shear and tensile faults in a half-space, Bull. seism. Soc. Am., 82, 1018–1040.

Van Opstal, The effect of Base-Rock Rigidity on Subsidence Due to Reservoir Compaction, Proc. 3rd Congr. Of the Int. Soc. Of Rock Mech., Denver II Part B p. 1102-1111, 1974.

Pijnenburg, R. P. J., Verberne, B. A., Hangx, S. J. T., & Spiers, C. J. (2018). Deformation Behavior of Sandstones From the Seismogenic Groningen Gas Field: Role of Inelastic Versus Elastic Mechanisms. Journal of Geophysical Research: Solid Earth, 123 (7), 5532-5558.

Pijnenburg, R. P. J., Hangx, S. J. T., & Spiers, C. J. (2019). Inelastic deformation of the Slochteren sandstone: Stress-strain relations and implications for induced seismicity in the Groningen gas field. *Journal of Geophysical Research: Solid Earth*, 124 (5), 5254-5282.

Petersson, N. A., and Sjögreen, B. High order accurate finite difference modeling of seismo-acoustic wave propagation in a moving atmosphere and a heterogeneous earth model coupled across a realistic topography. *Journal of Scientific Computing* 74, 1 (2018), 290–323.

Ringrose P.S., Mathieson A., Wright I., Selamac F., Hansen O., Bissell R., Saoula N., Midgley J., 2013, *Energy Procedia* 37 (2013) 6226– 6236

Ruiz, H., Lien, M., Vatshelle, M., Alnes, H., Haverl, M., Sørensen, H., 2020, Monitoring the Snøhvit gas field using seabed gravimetry and subsidence, SEG International Exposition and 90th Annual Meeting, Expanded Abstracts

Rutqvist J., Antonio P. Rinaldi, Frederic Cappa, Pierre Jeanne, Alberto Mazzoldi, Luca Urpi, Yves Guglielmi, Victor Vilarrasa, 2016, Fault activation and induced seismicity in geological carbon storage – Lessons learned from recent modeling studies, *Journal of Rock Mechanics and Geotechnical Engineering*, Volume 8, Issue 6, 2016, Pages 789-804, ISSN 1674-7755,

Sjögreen, B., and Petersson, N. A. A fourth order accurate finite difference scheme for the elastic wave equation in second order formulation. *Journal of Scientific Computing* 52, 1 (2012), 17–48.

Spiers, C. J., Hangx, S. J., & Niemeijer, A. R. (2017). New approaches in experimental research on rock and fault behaviour in the Groningen gas field. *Netherlands Journal of Geosciences*, 96(5), s55-s69.

van Thienen-Visser, K., Pruiksma, J. P., & Breunese, J. N. (2015). Compaction and subsidence of the Groningen gas field in the Netherlands. *Proceedings of the International Association of Hydrological Sciences*, 372, 367-373.

Tromp, J., Komattisch, D., and Liu, Q. Spectral-element and adjoint methods in seismology. *Communications in Computational Physics* 3, 1 (2008), 1–32.

Vandeweyer, V.P. *et al.*, 2021. Modelling the DAS response for offshore CO₂ storage sites, 15th International Conference on Greenhouse Gas Control Technologies, GHGT-15, 15th 18th March 2021 Abu Dhabi, UAE

De Waal, J. A. (1986). On the rate type compaction behaviour of sandstone reservoir rock. Doornhof, D. (1992). Surface subsidence in the Netherlands-the Groningen gas-field. *Geologie en Mijnbouw*, 71(2), 119-130.

Wang, H. F. *et al.* Ground motion response to an ml 4.3 earthquake using colocated distributed acoustic sensing and seismometer arrays. *Geophys. J. Int.* 213, 2020–2036 (2018).

van Wees J.D., Maarten Pluymaekers, Sander Osinga, Peter Fokker, Karin Van Thienen-Visser, Bogdan Orlic, Brecht Wassing, Dries Hegen, Thibault Candela, 3-D mechanical analysis of complex reservoirs: a

novel mesh-free approach, *Geophysical Journal International*, Volume 219, Issue 2, November 2019, Pages 1118–1130, <https://doi.org/10.1093/gji/ggz352>

Ziqiu Xue, Tetsuma Toshioka, Naoshi Aoki, Yoshiaki Kawabe, Daiji Tanase,, 2017, Research and Development of a Permanent OBC System for Time-lapse Seismic Survey and Microseismic Monitoring at the Offshore CO₂ Storage Sites, *Energy Procedia*, Volume 114, 2017, Pages 3778-3785, ISSN 1876-6102,